

# Influence of Hydrogen Sulfide Exposure on the Transport and Structural Properties of the Metal–Organic Framework ZIF-8

Akshita Dutta,<sup>†,⊥</sup> Nina Tymińska,<sup>‡,⊥</sup> Guanghui Zhu,<sup>§,⊥</sup> James Collins,<sup>||</sup> Ryan P. Lively,<sup>\*,§</sup> J. R. Schmidt,<sup>\*,‡</sup> and Sergey Vasenkov<sup>\*,†</sup>

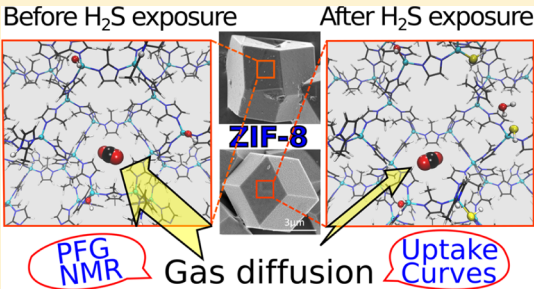
<sup>†</sup>Department of Chemical Engineering and <sup>||</sup>National High Magnetic Field Laboratory, University of Florida, Gainesville, Florida 32611, United States

<sup>‡</sup>Theoretical Chemistry Institute and Department of Chemistry, University of Wisconsin–Madison, 1101 University Avenue, Madison, Wisconsin 53706, United States

<sup>§</sup>School of Chemical and Biomolecular Engineering, Georgia Institute of Technology, 311 Ferst Drive NW, Atlanta, Georgia 30332, United States

## Supporting Information

**ABSTRACT:** The interaction between hydrogen sulfide and ZIF-8 was studied via structural characterizations and guest molecule diffusion measurements. It was found that hydrogen sulfide reacts with the ZIF-8 external particle surface to form a surface barrier that excludes the uptake of larger molecules (ethanol) and slows down the uptake of smaller molecules (carbon dioxide). Nonetheless, bulk transport properties were unaltered, as supported by pulsed field gradient nuclear magnetic resonance studies. Dispersion-corrected density functional theory calculations revealed that H<sub>2</sub>S is consumed by reactions occurring at the ZIF external surface. These reactions result in water and defect formation, both of which were found to be exothermic and independent of both crystallographic facets ( $\{001\}$  and  $\{110\}$ ) and surface termination. We concluded that these surface reactions lead to structural and chemical changes to the ZIF-8 external surface that generate surface barriers to molecular transport.



## INTRODUCTION

Hydrogen sulfide (H<sub>2</sub>S) is a toxic gas that is found in several industrial processes including petroleum refining, natural gas processing, biogas production, and wastewater treatment.<sup>1–6</sup> H<sub>2</sub>S is also a known poison for many transition-metal-based catalysts.<sup>7,8</sup> Metal–organic frameworks (MOFs) are promising porous materials for applications in catalysis, sorption, and separations involving natural gas, biogas, and crude oil or oil products. Because H<sub>2</sub>S can be present in fluid mixtures used in many of these applications, it is important to have a fundamental understanding of MOF–H<sub>2</sub>S interactions and their influence on the MOF transport and structural properties.

Some well-studied MOFs such as MIL-53 (Al, Cr, Fe), MIL-47, and MIL-100 (Cr) have been reported to show high sorption selectivity and chemical resistance to sulfur gases.<sup>9</sup> Among different types of MOFs, particular attention has been given to zeolitic imidazolate frameworks (ZIFs), a subset of MOFs that are topologically isomorphic with zeolites. The effects of H<sub>2</sub>S exposure on ZIF-8 has previously been studied by means of FT-IR, Raman, UV–vis–NIR, and X-ray powder diffraction (XRD).<sup>10</sup> The study demonstrated small perturbations of the ZIF-8 framework upon exposure to H<sub>2</sub>S at pressures of around 5–20 mbar in the surrounding gas phase. However, the exact nature of these perturbations remains unclear.

Herein, we examine the practical effects of these perturbations on guest transport in ZIF-8 and use a combination of experimental and computational approaches to provide insights into the atomistic nature of H<sub>2</sub>S-induced structural changes. Structural changes of ZIF-8 particles after H<sub>2</sub>S exposure were confirmed with scanning electron microscopy (SEM), N<sub>2</sub> physisorption, X-ray photoelectron spectroscopy (XPS), and X-ray diffraction (XRD). The guest transport properties of ZIF-8 particles before and after H<sub>2</sub>S exposure were measured with pulsed field gradient nuclear magnetic resonance (PFG NMR), gravimetric vapor uptake, and pressure decay gas uptake experiments. PFG NMR measurements of small molecule diffusion in ZIF-8 reveal no significant changes in the microscopic intraparticle diffusivities following prolonged exposure to H<sub>2</sub>S, indicating that the bulk transport properties of ZIF-8 are not noticeably modified by H<sub>2</sub>S. However, the gravimetric vapor uptake and pressure decay gas uptake experiments clearly show the formation of a surface barrier as a result of H<sub>2</sub>S exposure. This reaction was further confirmed by <sup>1</sup>H NMR and theoretical studies of H<sub>2</sub>S reactivity at the ZIF-8 surface.

Received: January 23, 2018

Revised: March 8, 2018

Published: March 9, 2018

## EXPERIMENTAL SECTION

**Materials.** All chemicals were purchased from Sigma-Aldrich and used without further purification. UHP N<sub>2</sub> was purchased from Airgas. An H<sub>2</sub>S gas mixture (5% H<sub>2</sub>S and 95% N<sub>2</sub> by weight) was purchased from Matheson.

**ZIF-8 Synthesis.** A sample of ZIF-8 used in the measurements was synthesized by modifying the procedure reported by Koros and co-workers.<sup>11</sup> A solution of 324 mg 2-methylimidazole and 538 mg sodium formate in 40 mL methanol was added to a solution of 588 mg Zn(NO<sub>3</sub>)<sub>2</sub>·6H<sub>2</sub>O in 40 mL methanol under vigorous magnetic stirring. The solution was heated to 363 K for 24 h in a sealed glass pressure vessel without stirring. The crystals were recovered by centrifugation and washed with methanol. The white powder was activated by keeping it at 383 K under vacuum for 12 h.

**Scanning Electron Microscopy.** Imaging of the crystal morphology was achieved using a Hitachi SU8230 cold field emission scanning electron microscope (CFE-SEM). The dry samples were attached to aluminum stubs using copper tape. The samples were then coated with a 2 nm layer of gold/palladium using a Hummer 6 gold/palladium sputterer. Imaging was taken at a working distance of 8 mm and a working voltage of 3 kV using a mix of upper and lower secondary electron detectors.

**Powder X-ray Diffraction.** Normal powder X-ray diffraction (PXRD) data were collected on a PANalytical X'Pert PRO multipurpose diffractometer in reflection Bragg–Brentano geometry operating with a Cu anode at 45 kV and 40 mA. Samples were mounted as loose powder onto a silicon zero background holder. PXRD patterns were collected with a step size of 0.02 degrees 2 $\theta$  and scan time of 10 s/step over 2–50 degrees 2 $\theta$ .

**N<sub>2</sub> Physisorption Analysis.** N<sub>2</sub> physisorption analysis was conducted with ultra-high-purity nitrogen at 77 K using a MicrotracBEL BELSORP-max instrument.

**X-ray Photoelectron Spectroscopy.** X-ray photoelectron spectra were recorded on a Thermo K-Alpha X-ray photoelectron spectrometer with Al K $\alpha$  radiation. Samples were evacuated overnight before being thinly layered onto carbon tapes as the internal standard.

**Preparation of ZIF-8 Samples Loaded with H<sub>2</sub>S and H<sub>2</sub>S-Exposed Samples.** The study of changes in structural and transport properties of ZIF-8 due to H<sub>2</sub>S exposure was performed by comparison of the properties of the ZIF-8 sample before and after its exposure to H<sub>2</sub>S. The sample exposure to H<sub>2</sub>S was performed as follows. Note that H<sub>2</sub>S is a highly toxic gas, and strict safety protocols must be followed to ensure safe handling of this gas. The following experimental protocols occur in a closed system within a fume hood, and all gases exiting that closed system are scrubbed to remove H<sub>2</sub>S. Approximately 100 mg of as-prepared ZIF-8 was loaded into a 5 mm medium-wall NMR tube (Wilmad Glass). The ZIF-8 sample in a tube was activated by keeping the sample at 383 K under vacuum for 12 h. A special gas manifold was built to safely handle the H<sub>2</sub>S mixture. A solution of 1 M NaOH was used as scrubber for the effluent. A poly(ethylenimine)-impregnated mesoporous silica (SBA-15) was synthesized and utilized as a solid scrubber for the vacuum line.<sup>12</sup> Upon activation, the ZIF-8 sample was loaded with H<sub>2</sub>S by exposing it to H<sub>2</sub>S/N<sub>2</sub> gas mixture (5% H<sub>2</sub>S and 95% N<sub>2</sub> by weight) at 0.9 atm for 8 h at 298 K. Following the sample exposure at 298 K, the sample temperature was briefly decreased down to around

77 K (by immersing the sample to liquid N<sub>2</sub> for 2–4 min) and increased again to around 298 K. This was done to maximize the H<sub>2</sub>S concentration, which, after the exposure to liquid N<sub>2</sub>, is expected to correspond to that on the desorption branch of the H<sub>2</sub>S adsorption isotherm for ZIF-8 at around 298 K. The NMR tube with the sample was then flame-sealed and kept for 22 days at 298 K. For <sup>1</sup>H magic angle spinning (MAS) PFG NMR studies, around 15 mg of ZIF-8 powder were introduced into 4 mm Pyrex MAS insert (Wilmad Glass). The <sup>1</sup>H PFG NMR and <sup>1</sup>H MAS PFG NMR studies of this sample were started one day after the sample preparation. The total duration of the measurements was around 5 days. Over this period, no changes in the measured data were observed. Following the 22 day H<sub>2</sub>S exposure, the sample was activated by keeping it under vacuum at 383 K for 12 h.

**Preparation of ZIF-8 Samples Loaded with CO<sub>2</sub> and C<sub>2</sub>H<sub>4</sub>.** To perform PFG NMR diffusion studies of probe molecules [single <sup>13</sup>C enriched CO<sub>2</sub> and C<sub>2</sub>H<sub>4</sub>, 99% isotopic purity (Sigma-Aldrich)] in the ZIF-8 samples, between 70 and 95 mg of as-prepared ZIF-8 or H<sub>2</sub>S-exposed ZIF-8 was introduced into a 5 mm medium-wall NMR tube (Wilmad Glass). An NMR tube containing the porous material was connected to a custom-made vacuum system and subjected to an activation under a high vacuum (<10<sup>-3</sup> Pa) at 383 K for 10 h. A desired mass of a selected sorbate was cryogenically condensed into the tube using liquid nitrogen. Following sorbate loading, the tube was flame-sealed and separated from the vacuum system. The concentration of each gas in the ZIF-8 NMR samples was determined by comparing the <sup>13</sup>C NMR signal of the adsorbed gas in these samples with the <sup>13</sup>C NMR signal in an NMR tube containing only pure gas at a known pressure, in the same way as discussed in our previous work.<sup>13</sup> These loadings in the as-prepared and H<sub>2</sub>S-exposed samples are reported in Table 1 and are comparable within the experimental error. This consistency allows for direct comparison of diffusion properties of each sorbate in the respective ZIF-8 samples.

**Table 1. Concentrations of Probe Molecules (Ethylene and Carbon Dioxide) in the As-Prepared and H<sub>2</sub>S-Exposed ZIF-8 Samples at 298 K as Determined Using <sup>13</sup>C NMR Signal Analysis**

sorbate	concentration in as-prepared ZIF-8 (mmol/g)	concentration in H <sub>2</sub> S-exposed ZIF-8 (mmol/g)
C <sub>2</sub> H <sub>4</sub>	2.5 ± 0.2	2.3 ± 0.2
CO <sub>2</sub>	2.4 ± 0.4	2.2 ± 0.2

**Pulsed Field Gradient Nuclear Magnetic Resonance.** The reported PFG NMR diffusion measurements were primarily performed using a 14 T AVANCE III spectrometer (Bruker BioSpin) operating at <sup>13</sup>C and <sup>1</sup>H resonance frequencies of 149.8 and 600 MHz, respectively. Complementary measurements were also performed using a 17.6 T AVANCE III HD spectrometer (Bruker BioSpin) operating at <sup>13</sup>C and <sup>1</sup>H resonance frequencies of 188.6 and 750 MHz, respectively. These complementary measurements were carried out to confirm that the reported diffusion data do not depend on the magnetic field strength used in the measurements. Sine-shaped, bipolar magnetic field gradients with the effective duration between 1.5 and 5.2 ms and amplitudes up to 20 T/m were generated using Diff50 or Diff30 diffusion probes (Bruker BioSpin). Selected diffusion studies were performed at 14 T

using a high-resolution MAS probe (Bruker BioSpin) with sine-shaped, bipolar magnetic field gradients, which have amplitudes up to 0.56 T/m. The MAS rate was 5 kHz. The reported NMR data were obtained after keeping the samples at 298 K for at least 12 h after the sorbate loading to ensure the sorption equilibrium conditions in the sample. It was verified that the measured NMR data do not depend on the time in the magnet after this initial equilibration.

Diffusion measurements were performed using the 13-interval PFG NMR pulse sequence with bipolar gradients,<sup>14</sup> modified by the addition of a longitudinal eddy current delay. The diffusivities were obtained from the measured PFG NMR attenuation curves, that is, dependencies of the PFG NMR signal intensity on the effective magnetic field gradient strength ( $g$ ) with all other pulse sequence parameters held fixed. PFG NMR signal intensities were obtained separately for carbon dioxide and ethylene by integration of the corresponding NMR spectra. Under our measurement conditions, the  $^{13}\text{C}$  NMR spectra of  $\text{CO}_2$  and  $\text{C}_2\text{H}_4$  exhibit single lines at around 125 and 123 ppm, respectively. The  $^1\text{H}$  NMR spectrum of  $\text{C}_2\text{H}_4$  consists of a single line at around 5 ppm. In the case of normal self-diffusion with a single diffusion coefficient ( $D$ ), PFG NMR attenuation curves can be presented as<sup>15</sup>

$$\Psi = \frac{S(g)}{S(g \approx 0)} = \exp(-Dq^2t) \quad (1)$$

where  $\Psi$  is the PFG NMR signal attenuation,  $S$  is the PFG NMR signal intensity,  $t$  is the time of observation of the diffusion process (i.e., diffusion time), and  $q = 2\gamma g\delta$ , where  $\gamma$  is the gyromagnetic ratio and  $\delta$  is the effective gradient pulse length. In the case of normal self-diffusion in three dimensions, the mean square displacement (MSD) is related to  $D$  and  $t$  by the Einstein relation

$$\langle r^2 \rangle = 6Dt \quad (2)$$

Longitudinal ( $T_1$ ) and transverse ( $T_2$ ) NMR relaxation times were estimated using the 13-interval PFG NMR sequence. For  $T_1$  relaxation times, the measurements were performed by changing the time interval between the second and third  $\pi/2$  radiofrequency pulses of the sequence while keeping all other time intervals constant. For  $T_2$  relaxation times, the measurements were performed by changing the time interval between the first and second  $\pi/2$  radiofrequency pulses of the sequence. Under the conditions of these measurements, the gradient amplitude was kept sufficiently small to ensure that the relaxation data were not perturbed by signal attenuation due to diffusion inside ZIF-8 crystals. At the same time, this gradient amplitude was sufficiently large to suppress all signals from the gas phase of the sample. As a result, the measured  $T_1$  and  $T_2$  relaxation times correspond to species located inside ZIF-8 crystals.

The primary technique for diffusion measurements of probe molecules (ethylene and carbon dioxide) in ZIF-8 samples was  $^{13}\text{C}$  PFG NMR at 14 T. The values of  $T_1$  and  $T_2$   $^{13}\text{C}$  NMR relaxation times measured at 14 T for these molecules are presented in Table 2. In all cases, the results of the measurements were consistent with the absence of any distribution over relaxation times.

#### Macroscopic Diffusion Measurement of Ethanol.

Diffusion of ethanol into ZIF-8 crystals before and after  $\text{H}_2\text{S}$  exposure was measured in a TA Instrument VTI-SA+ gravimetric sorption apparatus to probe the existence of surface

**Table 2.**  $T_1$  and  $T_2$   $^{13}\text{C}$  NMR Relaxation Times Measured at 14 T for Ethylene and Carbon Dioxide in ZIF-8 Samples

sorbate	$T_1$ $^{13}\text{C}$ NMR in as-prepared ZIF-8 (ms)	$T_1$ $^{13}\text{C}$ NMR in $\text{H}_2\text{S}$ -exposed ZIF-8 (ms)	$T_2$ $^{13}\text{C}$ NMR in as-prepared ZIF-8 (ms)	$T_2$ $^{13}\text{C}$ NMR in $\text{H}_2\text{S}$ -exposed ZIF-8 (ms)
$\text{C}_2\text{H}_4$	$320 \pm 50$	$360 \pm 50$	$13 \pm 2$	$14 \pm 2$
$\text{CO}_2$	$200 \pm 30$	$260 \pm 30$	$20 \pm 3$	$12 \pm 2$

barriers resulting from the exposure. The device allows continuous monitoring of the mass gain in samples exposed to specific relative saturation (RS) by a high-precision microbalance (accuracy  $\pm 10 \mu\text{g}$ ) to which the sample holder is suspended. The material in the chamber is exposed to RS steps via a controlled flow of a mixture of dry and wet gases, where the wet gas is generated by flowing nitrogen through a temperature-controlled saturation chamber of ethanol. Approximately 15 mg samples were used for these analyses. Before the introduction of organic vapor, the sample was activated until a constant mass was observed at 120 °C and 0% RS. Uptake was measured at 35 °C at a relative saturation of 0.5.

**Pressure Decay Adsorption Measurement of  $\text{CO}_2$  and  $\text{CH}_4$ .** Diffusion of  $\text{CO}_2$  gas molecules into ZIF-8 crystals was measured in a home-built dual-volume pressure decay cell. Around 20 mg of the activated sample was loaded in the sample cell. The sample was activated again in the sample cell at 90 °C overnight under dynamic vacuum. The system was then cooled down to 35 °C for diffusion measurements.  $\text{CO}_2$  was dosed into the chamber to a predetermined pressure. The pressure drop in the sample cell was recorded and transformed to uptake curves. Because the sample sizes before and after  $\text{H}_2\text{S}$  exposure are essentially the same and we expect no major heat effects, we believe that the transport rates can be qualitatively compared between the samples by comparing the  $\text{CO}_2$  uptake curves. The quantitative analysis of the curves was prevented by the existence of a broad distribution over sizes of ZIF-8 particles in the sample. In addition to the  $\text{CO}_2$  uptake curves, the pressure decay cell was used to measure the uptake capacity for  $\text{CH}_4$ . Adsorption of  $\text{CO}_2$  and  $\text{CH}_4$  was measured on the same sample (i.e., pre- and post- $\text{H}_2\text{S}$  exposure) after reactivation in the pressure decay cell. The uptake capacity points were calculated from the pressure drop in the dosing volume and the equilibrium pressure in the sample volume.

**Computational Investigation: DFT Studies of  $\text{H}_2\text{S}$  Reactivity.** Dispersion-corrected density functional theory (DFT-D) with a 600 eV energy cutoff and a projector-augmented wave treatment of core electrons<sup>16</sup> at the PBE+D3<sup>17,18</sup> level of theory was used to calculate the energetics of possible reactions between  $\text{H}_2\text{S}$  and ZIF-8 via periodic code Vienna Ab initio Simulation Package (VASP).<sup>19–22</sup> The  $k$ -space was sampled at the  $\Gamma$ -point with convergence criteria of  $10^{-5}$  eV and 0.03 eV/Å for total energy and ionic force, respectively. The initial structure of ZIF-8 was obtained from the crystallographic data provided in the Cambridge Structural Database.<sup>23</sup> During geometrical optimization, the lattice constant of a cubic unit cell (containing 12-Zn, 48-N, 96-C and 120-H atoms) was kept fixed at the experimental value of 16.991 Å.<sup>23</sup> This can be done because the concentration of defects in bulk is expected to be low.<sup>24</sup> The PBE+D3 optimized structure of bulk ZIF-8 was used to create surface models by cleaving Zn–N bonds crossing either [001] or [110] crystal plane and inserting a vacuum gap of  $\sim 20$  Å between periodic images. The positions of the top two Zn layers in these slabs were allowed to relax, whereas those at the



bottom layer were kept fix at the bulk positions. Dipole interactions between periodic images of such asymmetric slabs were eliminated via dipole corrections applied in all surface calculations.

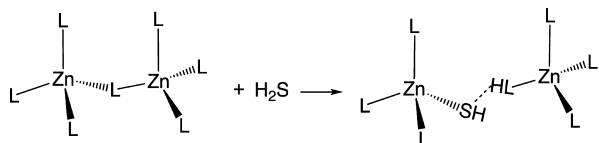
A variety of surface-terminating groups, including (but not limited to) 2-methylimidazole (HmIM), OH groups, and/or water may be present at the outer surface of ZIFs, depending on the conditions.<sup>25–30</sup> For simplicity, we model outer surfaces of ZIFs by capping exposed (undercoordinated) Zn<sup>2+</sup> with those species.<sup>31–34</sup> In particular, we considered two mixed surface terminations: (i) HmIM/OH where half of undercoordinated Zn<sup>2+</sup> ions are capped with OH groups and the other half by HmIM and (ii) H<sub>2</sub>O/OH, with water molecules instead of HmIM.

Reaction energies were calculated as energy differences between product(s) and reactant(s). For example, dangling linker formation reaction energy ( $\Delta E_{\text{rxn,DL}}$ ) was calculated as

$$\Delta E_{\text{rxn,DL}} = E_{\text{ZIF,DL}} - E_{\text{ZIF}} - E_{\text{HX}} \quad (3)$$

where  $E_{\text{ZIF,DL}}$ ,  $E_{\text{ZIF}}$ , and  $E_{\text{HX}}$  are energies of a defective ZIF-8 unit cell, a pristine ZIF-8 unit cell, and an isolated reactant (e.g. H<sub>2</sub>S) molecule, respectively (see Scheme 1);  $\Delta E_{\text{rxn,DL}}$  for the

**Scheme 1.** H<sub>2</sub>S Insertion into Zn–N Bond of ZIF-8 Bulk in the Dangling Linker Formation Reaction<sup>a</sup>



<sup>a</sup>L denotes 2-methylimidazolate.

corresponding reaction at the external surface is calculated in a similar fashion. Reaction barriers were obtained as a difference between the energy of the interacting reactants and the transition state found by the climbing image nudged elastic band (cNEB)<sup>35,36</sup> method as implemented in VASP.

Additional details on the computational investigation and surface models can be found in the Supporting Information.

## RESULTS AND DISCUSSION

SEM images of single crystals of ZIF-8 samples before and after H<sub>2</sub>S exposure are shown in Figure 1. A portion of the H<sub>2</sub>S-exposed crystals showed uniform pinholes on the surface, indicating possible reaction of H<sub>2</sub>S with the ZIF-8 crystals. Sizes of single crystals in the as-prepared sample were found to be similar to those in the H<sub>2</sub>S-exposed ZIF-8 sample (Figure S1 and Table S1). It is seen in Figure S2 that crystals in both samples form aggregates. The aggregate sizes were observed to be as large as 47 μm. No noticeable changes in the aggregate sizes were observed as a result of the sample exposure to H<sub>2</sub>S.

The crystallinity of ZIF-8 samples before and after H<sub>2</sub>S exposure was checked with XRD. Figure 2 compares the XRD patterns of the as-prepared and H<sub>2</sub>S-exposed ZIF-8 samples. These patterns provide evidence of changes in the structure of ZIF-8 due to H<sub>2</sub>S exposure. The appearance of the broad features that are seen in the pattern of the H<sub>2</sub>S-exposed ZIF-8 is attributed to an amorphization of a fraction of the sample. However, the majority of the sample appears to have the same structure as that of as-prepared ZIF-8, as judged from an overlap of the narrow reflections recorded for both samples.

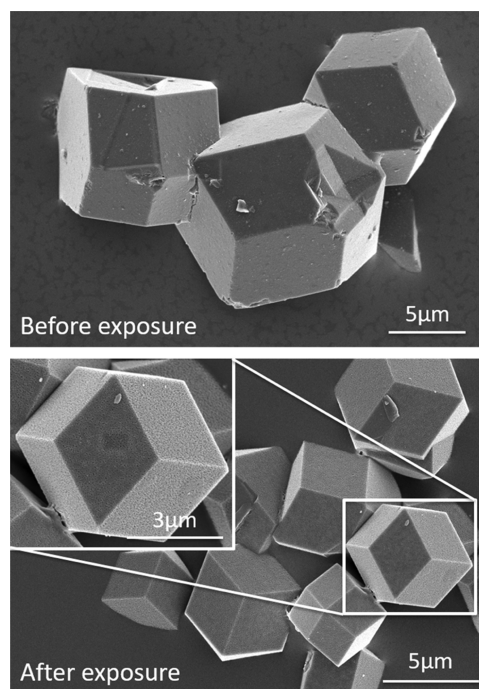


**Figure 1.** SEM images of ZIF-8 samples before and after H<sub>2</sub>S exposure. Both samples show agglomeration of individual single crystals.

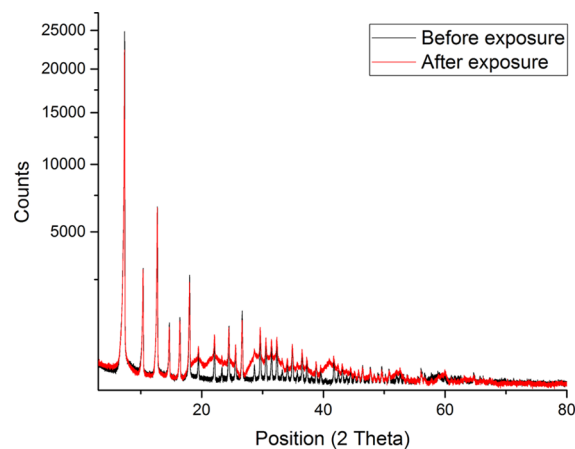


**Figure 2.** XRD patterns of ZIF-8 samples before and after H<sub>2</sub>S exposure.

Indeed, the percentage of decrease in relative crystallinity of this material depends on the conditions to which ZIF-8 is exposed. For instance, prior experimental studies have shown that ZIF-8 degrades significantly upon prolonged exposure to humid SO<sub>2</sub>.<sup>37,38</sup> In combined experimental and computational investigation by Pang et al.,<sup>31</sup> these authors concluded that the (100) surface is more stable than the (110) surface against SO<sub>2</sub>-induced degradation. Han et al.<sup>33</sup> performed computational study on stability of ZIFs in humid acidic environments. They compared the reaction energies for the formation of a dangling linker (a type of point defect) with various acid gases (including H<sub>2</sub>S) in pristine bulk and at the (001) surface of ZIF-8 and ZIF-2 terminated by water molecules. Such defects potentially lead to the degradation of ZIFs, which is expected to be accelerated in the presence of acid gases and water (see Scheme 1). Such a mechanism was first proposed by Zhang et al.<sup>24</sup>

Nitrogen physisorption isotherms for each sample are shown in Figure 3. The small alteration in the structure of ZIF-8 upon

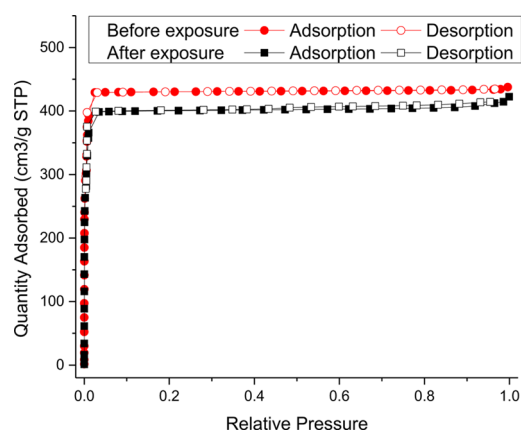


**Figure 3.** N<sub>2</sub> adsorption isotherms measured at 77 K for the as-prepared and H<sub>2</sub>S-exposed ZIF-8 samples.

H<sub>2</sub>S exposure, as noted by XRD, manifests in slight differences in the N<sub>2</sub> adsorption isotherms. Table 3 shows the corresponding surface area and pore volume for the as-prepared and H<sub>2</sub>S-exposed ZIF-8 samples. Quantitatively, there

**Table 3. Surface Area and Pore Volumes Obtained for the As-Prepared and H<sub>2</sub>S-Exposed ZIF-8 Samples from the Analysis of the Nitrogen Adsorption Isotherms**

sample	BET surface area (m <sup>2</sup> /g)	micropore area (m <sup>2</sup> /g) <i>t</i> -plot	pore volume (cm <sup>3</sup> /g)	micropore volume (cm <sup>3</sup> /g) <i>t</i> -plot
as-prepared ZIF-8	1837	1826	0.67	0.66
H <sub>2</sub> S-exposed ZIF-8	1684	1670	0.65	0.61

is a small (around 8%) decrease in the micropore surface area and volume following the H<sub>2</sub>S exposure. A smaller difference in the total pore volume in comparison with the micropore volume was observed because of the H<sub>2</sub>S exposure (Table 3). This result can be explained by the conversion of a fraction of micropores of ZIF-8 into larger pores, although the mechanism for this conversion remains unclear.

XPS was used to examine the surface of the ZIF-8 particles. Figure 4 shows the Zn 2p, O 1s, N 1s, and S 2p spectra before and after H<sub>2</sub>S exposure. All spectra were normalized to the magnitude of Zn 2p<sub>3/2</sub> peak; hence, the changes in intensity of other elements indicate the amount changed relative to Zn. After exposure to H<sub>2</sub>S, S 2p peaks are observed, indicating that nonlabile sulfur species are present on the crystal surface. In addition, the O 1s peak intensity has dropped after the exposure, suggesting that oxygen species were removed during the exposure. The XPS spectra indicate the possible substitution reactions between H<sub>2</sub>S and the surface oxygen groups (most likely to be terminating hydroxyl groups); computational evidence for the plausibility of such reactions is discussed below.

Figure 5 presents the examples of the <sup>13</sup>C PFG NMR attenuation curves measured at 14 T for the probe molecules (ethylene and carbon dioxide), which were used to assess the transport properties of the as-prepared and H<sub>2</sub>S-exposed ZIF-8

samples. This figure also shows additional attenuation curves, which were measured under the same conditions using <sup>1</sup>H PFG NMR at 14 T (labeled as <sup>1</sup>H in the figure) and using <sup>13</sup>C PFG NMR at 17.6 T (labeled as 188.6 MHz in the figure). The good agreement between the attenuation curves measured at different fields (for carbon dioxide) or using different nuclei (for ethylene) and otherwise the same conditions confirms the absence of any measurement artifacts in our data. The attenuation curves are essentially mono-exponential, that is, linear in the presentation of Figure 5, in agreement with eq 1.

For each sample, the attenuation curves were measured at different diffusion times, as indicated in the figure. In the presentation of Figure 5, the attenuation curves measured at different diffusion times are expected to coincide if the diffusion coefficient does not change with the diffusion time (eq 1). Hence, the coincidence of the data in Figure 5 observed for each sorbate and sample type indicates the time-independence of the measured diffusivities. Likewise, a good agreement between the attenuation curves measured for each sorbate in the as-prepared and H<sub>2</sub>S-exposed ZIF-8 shows that the measured diffusivity is not influenced by the H<sub>2</sub>S exposure. Because of the coincidence of the attenuation data, a single mono-exponential least squares fit was used for each sorbate (Figure 5). The resulting best fit diffusivities are equal to  $(1.1 \pm 0.2) \times 10^{-10}$  and  $(3.1 \pm 0.5) \times 10^{-10}$  m<sup>2</sup>/s for ethylene and carbon dioxide, respectively. These diffusivities are in satisfactory agreement with the corresponding diffusion coefficients measured previously by PFG NMR for ethylene and carbon dioxide in ZIF-8 under similar experimental conditions.<sup>39,40</sup>

Although H<sub>2</sub>S exposure resulted in noticeable changes of structural properties of ZIF-8 (Figures 1–4), our PFG NMR data show that the bulk ZIF-8 transport properties remain unchanged within the experimental uncertainty. It is important to note that in the case of three-dimensional site percolation, a partial or complete blockage of only about 8% of all sites is not expected to lead to a significant change in the diffusivity if the blocked sites are distributed more or less randomly.<sup>41</sup> However, the gravimetric ethanol uptake measurement shown in Figure 6 indicated that larger molecules, such as ethanol, are excluded from the ZIF-8 particles after H<sub>2</sub>S exposure, in contrast to pristine ZIF-8. Combining the PFG NMR data with the macroscopic diffusion data, these results can be explained by assuming that structural changes caused by the exposure to H<sub>2</sub>S mostly occur at or near the external surface of ZIF-8 aggregates.

Further measurement of guest transport properties was carried out with CO<sub>2</sub> using the pressure decay method. Because of transducer sensitivity limitations, the pressure in the sample cell was dosed in one-step to 2.0 bar in this case. The qualitative trends of CO<sub>2</sub> diffusion into the samples are shown in Figure 7. We observed that CO<sub>2</sub> diffusion into the ZIF-8 samples after H<sub>2</sub>S exposure was reduced compared to CO<sub>2</sub> diffusion into pristine ZIF-8 samples. These results suggest that the reaction of H<sub>2</sub>S with ZIF-8 results in the formation of a surface barrier that excludes larger molecules such as ethanol and retards transport of smaller molecules such as CO<sub>2</sub>. It was also observed that the CO<sub>2</sub> and CH<sub>4</sub> uptake capacities are slightly (by 10–15%) increased because of the exposure to H<sub>2</sub>S (Figure S3). In particular, the CO<sub>2</sub> uptake increased from 1.03 mmol/g to 1.18 mmol/g at 1.28 bar after the exposure. We attribute the observed small increase in the CO<sub>2</sub> and CH<sub>4</sub> uptake to additional interactions in the lattice locations affected by the exposure to H<sub>2</sub>S.

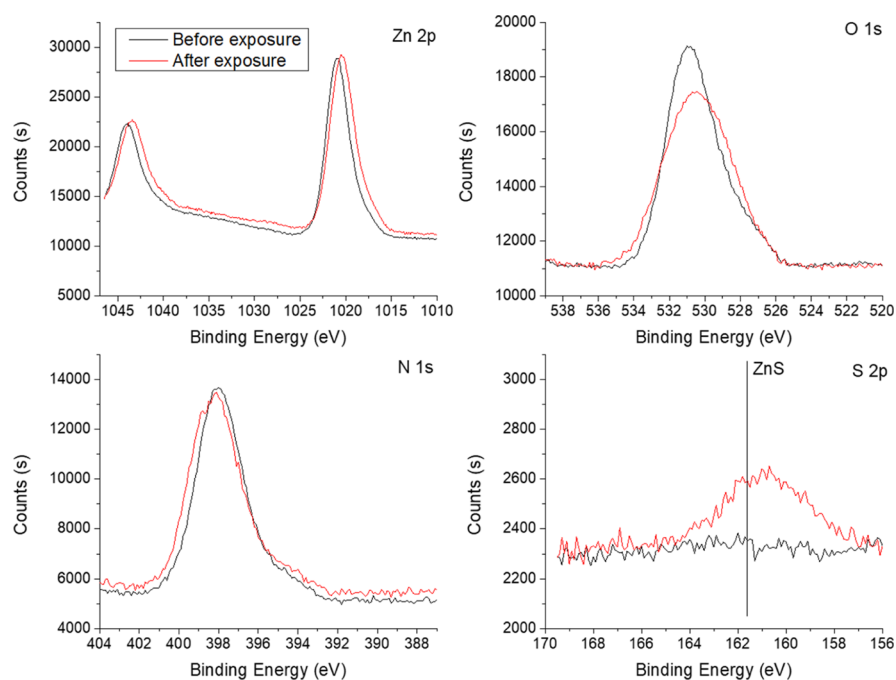


**Figure 4.** High-resolution X-ray photoelectron spectra for the Zn 2p, O 1s, N 1s, and S 2p binding energy regions for ZIF-8 samples before and after H<sub>2</sub>S exposure. Spectra have been shifted based on carbon 1s as an internal standard.

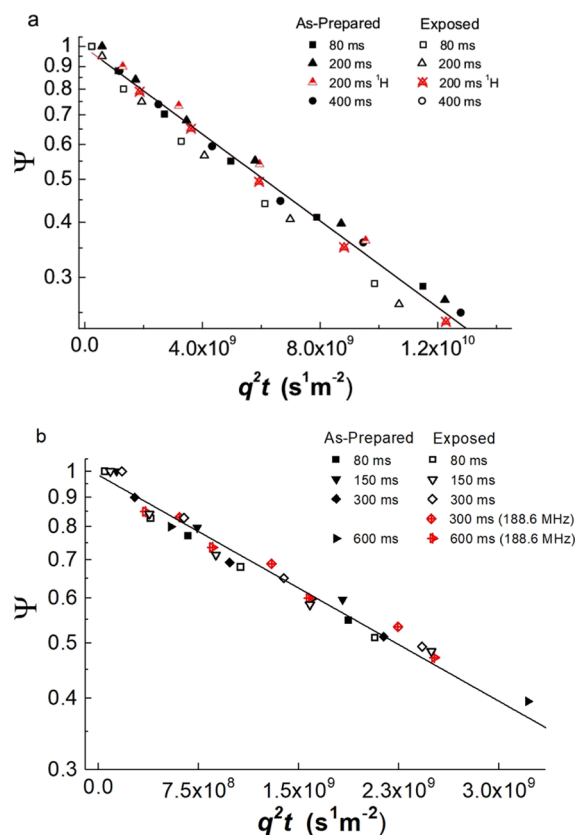


**Figure 5.** PFG NMR attenuation curves measured for (a) ethylene and (b) carbon dioxide in the as-prepared and H<sub>2</sub>S-exposed ZIF-8 samples at 298 K using the 13-interval PFG NMR sequence.

These experimental conclusions are also consistent with our computational results, which suggest significant reactivity for ZIF surfaces with H<sub>2</sub>S, regardless of the surface termination. For example, the dangling linker formation reaction energy

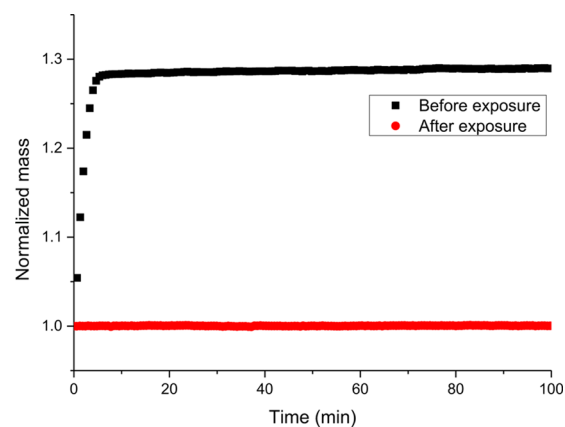


**Figure 6.** Uptake curves of ethanol into ZIF-8 crystals before and after H<sub>2</sub>S exposure.

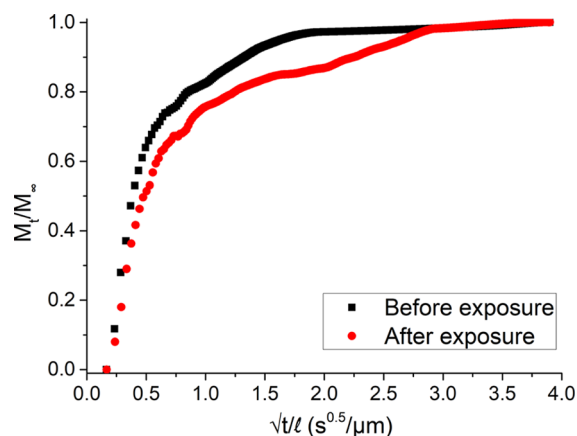


**Figure 7.** Normalized uptake curves of CO<sub>2</sub> in the ZIF-8 samples before and after H<sub>2</sub>S exposure.



( $\Delta E_{\text{rxn,DL}}$ , see eq 3) with  $\text{H}_2\text{S}$  at the {001} facet (with a  $\text{H}_2\text{O}/\text{OH}$  termination) is  $-18.0$  kcal/mol and it is more exothermic (by about 11 kcal/mol) than dangling linker formation via reaction with water. Similar results are found for other facets/surface terminations; see Table S2 in the Supporting Information. This degradation also proceeds with moderate barriers, for example,  $\sim 11.9$  kcal/mol for the aforementioned case. Our results are also consistent with previous computational studies<sup>31,33,37,38</sup> showing that the external surfaces of ZIFs are more prone to degradation than the bulk and that this process is enhanced in presence of acid gases compared to water. For instance, Han et al.,<sup>33</sup> calculated  $\Delta E_{\text{rxn,DL}}$  for the reaction between  $\text{H}_2\text{S}$  and bulk ZIF-8, which was found to be less exothermic by about 22 kcal/mol than that on the (001) water-passivated surface.

It is important to note that the maximum diffusion times used in the reported above PFG NMR measurements were limited by the  $T_1$  NMR relaxation times (Table 2). Hence, it was not technically possible to perform PFG NMR measurements at the diffusion times, which are so large that the molecular MSDs become similar to the aggregate sizes and, as a result, are influenced by the external aggregate surface. Such influences can either increase (in the case of no transport barriers at the surface) or decrease (in the case when such barriers are present) the values of the measured MSDs and the corresponding diffusivities,<sup>15</sup> which would be manifested in the changes of the attenuation curves in Figure 5 with increasing diffusion time. The absence of such changes in the figure indicates that larger diffusion times are required for observation of surface transport barriers by PFG NMR. Our PFG NMR data show no changes in the intra-ZIF diffusivity for two very different sorbate molecules ( $\text{C}_2\text{H}_4$  and  $\text{CO}_2$ ). Hence, no changes in the diffusion selectivity due to  $\text{H}_2\text{S}$  exposure are expected when the transport is controlled by intra-ZIF diffusion, that is, when crystals are sufficiently large. However, when the transport rate is controlled by surface transport barriers some changes in diffusion selectivity are possible, but these are difficult to control. Hence, this case is not expected to be relevant for applications.

It was attempted to investigate the diffusion of  $\text{H}_2\text{S}$  and/or products of  $\text{H}_2\text{S}$  reaction with the ZIF-8 framework using  $^1\text{H}$  PFG NMR at 14 T in the ZIF-8 samples, which were loaded with a small amount of  $\text{H}_2\text{S}$  as discussed in the experimental section. A baseline distortion due to magnetic susceptibility effects prevented us from seeing any NMR lines in the spectra acquired using a single radiofrequency pulse even after several hours of signal accumulation.

The baseline distortions were significantly reduced when using the 13-interval  $^1\text{H}$  PFG NMR sequence with a longitudinal eddy current delay and the small gradient strength of 0.3 T/m. Under these measurement conditions, only species diffusing in the gas phase of the sample with diffusivities in the range of  $10^{-8}$   $\text{m}^2/\text{s}$  or larger can be significantly attenuated by the sequence. Application of this sequence to the as-prepared ZIF-8 sample after activation (viz., the reference sample) and the ZIF-8 sample loaded with  $\text{H}_2\text{S}$  after activation (viz. the  $\text{H}_2\text{S}$  sample) revealed a single broad line at around 4.9 ppm (Figure 8), which was present in the  $\text{H}_2\text{S}$  sample and absent in the reference sample. This line is in the range of OH groups. It may originate from some preexisting OH groups, that is, surface OH groups, which become more mobile because of the reaction with  $\text{H}_2\text{S}$ . A higher mobility of such species in the  $\text{H}_2\text{S}$  sample can make them observable by  $^1\text{H}$  NMR. We tentatively assign

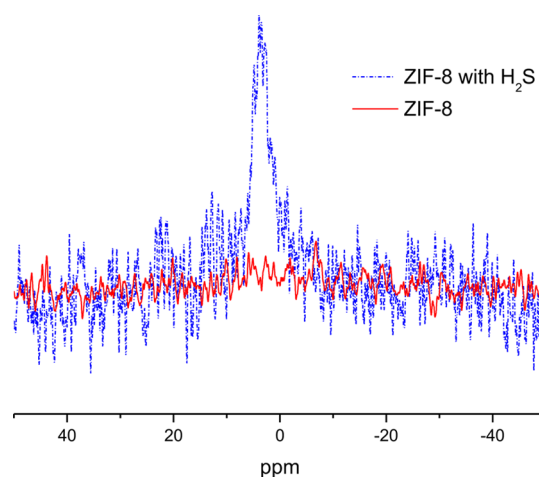


**Figure 8.**  $^1\text{H}$  NMR spectra measured with the 13-interval PFG NMR sequence at 298 K in the following two samples: reference sample (solid line), and  $\text{H}_2\text{S}$  sample (dotted line). The measurements were performed using the small gradient of 0.3 T/m, which ensures that under the measurement conditions only species diffusing in the gas phase of the sample with diffusivities around  $10^{-8}$   $\text{m}^2/\text{s}$  or larger can be significantly attenuated by the sequence.

the line at 4.9 ppm to a small amount of water molecules formed as a result of a reaction of  $\text{H}_2\text{S}$  with surface OH groups (vide infra).

The  $T_1$  and  $T_2$   $^1\text{H}$  NMR relaxation times of this water line were estimated to be 1.3 s and 5.6 ms, respectively.  $^1\text{H}$  PFG NMR diffusion measurements of the water molecules corresponding to the line at 4.9 ppm showed no signal attenuation even when the largest gradient strength (10 T/m), largest duration of the gradient pulse (5.2 ms), and largest diffusion time (0.5 s) were used (Figure S4). This result indicates the diffusivity of around  $5 \times 10^{-15}$   $\text{m}^2/\text{s}$  or less at 298 K. A possible explanation of these results is provided below. Complementary studies performed at 17.6 T showed qualitatively the same results: no PFG NMR signal attenuation was observed even when the largest gradient strength (19 T/m), largest duration of the gradient pulse (4.5 ms), and largest diffusion time (40 ms) were used. The diffusion time at 17.6 T was lower than that at 14 T because of a lower signal-to-noise ratio observed at a former field strength. Because of the lower diffusion time used at 17.6 T, the upper limit of the diffusivity reported above was not improved (i.e., decreased) as a result of the complementary measurements at 17.6 T.

The  $^1\text{H}$  PFG NMR data discussed above indicate that the water molecules associated with the line at 4.9 ppm are either completely immobile or diffuse many orders of magnitude slower than water in ZIF-8 when a significant fraction of the ZIF-8 micropore volume is filled with water. In the latter case, the water diffusivity is expected to be around  $10^{-11}$   $\text{m}^2/\text{s}$  or higher at 298 K.<sup>42</sup> The water diffusivity of around  $5 \times 10^{-15}$   $\text{m}^2/\text{s}$  or less at 298 K may result from diffusion over strong adsorption sites or defects in the ZIF-8 framework. Such diffusion is expected under the conditions of an extremely low water concentration, which can be comparable with the concentration of strong adsorption sites or defects. The slow mobility and strong interaction with the ZIF-8 framework of the species corresponding to the line at 4.9 ppm were confirmed by the following observation. It was found that the NMR spectrum measured under the same conditions as those in Figure 8 after opening the  $\text{H}_2\text{S}$  sample and activation of this

sample under a high vacuum at 383 K for 10 h still shows the line at approximately the same ppm value, but the intensity of this line is reduced by a factor of around 3 in comparison with the corresponding line in the H<sub>2</sub>S sample (Figure S5).

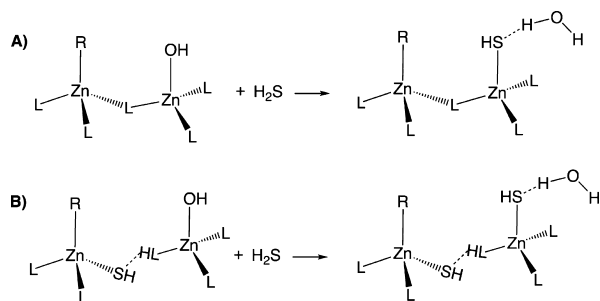
MAS is often used in NMR to decrease the line width and improve the spectral resolution. MAS PFG NMR has been demonstrated to successfully study self-diffusion of single and multicomponent sorbates in zeolites and MOFs under conditions when traditional PFG NMR measurements suffer from line broadening because of restricted molecular mobility in micropores.<sup>40,43,44</sup> The main disadvantage of MAS PFG NMR is more than an order of magnitude smaller maximum gradient strength in comparison with conventional PFG NMR. An application of MAS PFG NMR allowed observing fast diffusing species contributing to the line at around 4.9 ppm. The diffusivity of these species is around  $3 \times 10^{-9}$  m<sup>2</sup>/s (Figure S6), which can be tentatively assigned to confined water in exchange with water in the gas phase of the sample or diffusion of water in the part of the ZIF-8 sample destroyed by reactions with H<sub>2</sub>S. This diffusivity was not observed using PFG NMR without MAS because of the significant line broadening and short *T*<sub>1</sub> relaxation time (8 ms). Molecular H<sub>2</sub>S is expected to have a chemical shift in the range between around 0 and 2 ppm.<sup>45</sup> We have not observed an NMR line in this range in the H<sub>2</sub>S-loaded samples using MAS NMR or MAS PFG NMR (5 kHz MAS rate). This result can be explained by a dissociative adsorption of H<sub>2</sub>S leading to the formation of water or other species containing OH groups with the diffusivities reported above. SH<sup>-</sup> anions, which are expected to have resonance at around -3 ppm,<sup>45</sup> were also not observed by MAS NMR or MAS PFG NMR under our experimental conditions. It is likely that a residual line broadening and low concentration of the SH<sup>-</sup> anion line prevented the observation of these anions in the studied samples.

The generation of water via ZIF surface reactions with H<sub>2</sub>S is supported from our DFT-D calculations, which shows that water formation resulting from the reaction between H<sub>2</sub>S and the surface OH groups

$$\Delta E_{\text{rxn},\text{H}_2\text{O}} = E_{\text{ZIF-SH}\cdot\text{H}_2\text{O}} - E_{\text{ZIF-OH}} - E_{\text{H}_2\text{S}}$$

at the (110) and (001) surfaces of ZIF-8 (illustrated in Scheme 2) is strongly exothermic, independent of the details of surface termination. However, this reaction is more exothermic at the (110) surface [ $\Delta E_{\text{rxn},\text{H}_2\text{O}}(110) = -35.2$  kcal/mol] than at the

**Scheme 2. Water Formation at the ZIF-8 Surfaces Terminated with OH and R Groups, Where the Latter is Either Water or HmIM<sup>a</sup>**



<sup>a</sup>H<sub>2</sub>S reaction with the OH group on a perfect surface is shown in panel A and with defective (where one of Zn–N bonds has been broken during prior reaction with H<sub>2</sub>S) in panel B.

(001) surface [ $\Delta E_{\text{rxn},\text{H}_2\text{O}}(001) = -28.5$  kcal/mol] of the material. These conclusions are unaltered via the presence of existing surface point defects (i.e., dangling linker): the water formation reaction becomes only slightly less exothermic in comparison to the defect-free surface (with all surface Zn–N bonds intact, as shown in panel A of Scheme 2). On the basis of the strong exothermic nature of all of the calculated  $\Delta E_{\text{rxn},\text{H}_2\text{O}}$  values (see Table S3), it can be assumed that the associated kinetic barriers are modest. To support this assumption, we performed proof-of-concept cNEB calculations on the perfect (001) surface with OH/H<sub>2</sub>O termination. No kinetic barrier was found for the water formation at this surface at the PBE+D3 level of theory. These computational results suggest that H<sub>2</sub>S may be consumed via facile surface reactions, resulting in the formation of free or surface bound water as well as point defects as discussed earlier in the text. In contrast, the reaction of bulk ZIF-8 with H<sub>2</sub>S to form dangling linkers (see Scheme 1) has about 10 times higher kinetic barrier as compared to the (001) hydrated surface ( $\sim 3.5$  vs  $\sim 30$  kcal/mol<sup>33</sup>), suggesting a much higher surface versus bulk reactivity of ZIFs with H<sub>2</sub>S.

Although no direct measurement of H<sub>2</sub>S diffusion in ZIF-8 could be performed, our computational results can provide insights into the transport properties of H<sub>2</sub>S in bulk, pristine ZIF-8. Using a combination of molecular dynamics simulations and transition state theory hopping rates (see Supporting Information), we estimate the infinite-dilution self-diffusion coefficient (*D*<sub>self,i</sub>) for H<sub>2</sub>S in ZIF-8 to be  $3.23 \pm 0.2 \times 10^{-10}$  m<sup>2</sup>/s at room temperature (25 °C). Hence, one can expect that this acid would diffuse through the pristine (defect free) bulk at the moderate rate. However, as H<sub>2</sub>S is likely to be consumed by ZIF-8 in reactions such as water or dangling linker formation, calculated *D*<sub>self,i</sub> reflecting diffusion of unreacted H<sub>2</sub>S validates that the diffusivity measured by PFG NMR for the line at 4.9 ppm should not be associated with the acid. For more information on computational details of H<sub>2</sub>S diffusivity simulations, see the Supporting Information.

## CONCLUSIONS

We applied a combination of experimental and computational approaches to provide insights into the interactions between H<sub>2</sub>S and ZIF-8. ZIF-8 crystals showed partial amorphization, surface morphological changes, surface chemical composition alteration, and decrease in the surface area after H<sub>2</sub>S exposure. The transport properties of ZIF-8 particles were also measured before and after H<sub>2</sub>S exposure. PFG NMR measurements of C<sub>2</sub>H<sub>4</sub> and CO<sub>2</sub> diffusion in ZIF-8 reveal no significant changes in the microscopic diffusivities following prolonged exposure to H<sub>2</sub>S. This observation indicates that the transport properties of bulk ZIF-8 are not noticeably modified by H<sub>2</sub>S. In contrast, gravimetric vapor uptake and pressure decay gas uptake experiments clearly show the formation of a surface barrier as a result of H<sub>2</sub>S exposure. The reaction between the ZIF-8 and H<sub>2</sub>S acid was further confirmed by <sup>1</sup>H NMR and computational investigation of H<sub>2</sub>S reactivity at the external surface of this material. These computational results suggest that H<sub>2</sub>S is consumed in the reaction with OH groups at the ZIF-8 external surfaces leading to water formation in an exothermic and effectively barrierless reaction. This work thus provides a framework for evaluating the MOF degradation as a result of acid gas exposure and represents a first observation of surface barrier formation in MOF materials due to chemical modification.



## ■ ASSOCIATED CONTENT

## S Supporting Information

The Supporting Information is available free of charge on the ACS Publications website at DOI: 10.1021/acs.jpcc.8b00798.

Additional experimental data and details on computational methods and models used in this study and detailed description of H<sub>2</sub>S diffusion in pristine ZIF-8 simulations including force field validation (PDF)

## ■ AUTHOR INFORMATION

## Corresponding Authors

\*E-mail: ryan.lively@chbe.gatech.edu (R.P.L.).

\*E-mail: schmidt@chem.wisc.edu (J.R.S.).

\*E-mail: vase17@ufl.edu (S.V.).

## ORCID

Nina Tymiąńska: 0000-0001-6988-5917

Guanghai Zhu: 0000-0002-7928-1129

Ryan P. Lively: 0000-0002-8039-4008

J. R. Schmidt: 0000-0002-1438-117X

Sergey Vasenkov: 0000-0002-8619-0612

## Author Contributions

<sup>†</sup>A.D., N.T., and G.Z., contributed equally to this work.

## Notes

The authors declare no competing financial interest.

## ■ ACKNOWLEDGMENTS

This work was supported as part of UNCAGE-ME, an Energy Frontier Research Center funded by the U.S. Department of Energy, Office of Science, Basic Energy Sciences under award # DE-SC0012577. This work was performed in part at the Georgia Tech Institute for Electronics and Nanotechnology, a member of the National Nanotechnology Coordinated Infrastructure, which is supported by the National Science Foundation (grant ECCS-1542174). A portion of this work was performed in the McKnight Brain Institute at the National High Magnetic Field Laboratory's AMRIS Facility, which is supported by the National Science Foundation Cooperative agreement no. DMR-1157490 and the State of Florida.

## ■ REFERENCES

- (1) Zhang, L.; De Schryver, P.; De Gussem, B.; De Muyenck, W.; Boon, N.; Verstraete, W. Chemical and Biological Technologies for Hydrogen Sulfide Emission Control in Sewer Systems: A Review. *Water Res.* **2008**, *42*, 1–12.
- (2) Ruddy, D. A.; Schaidle, J. A.; Ferrell, J. R.; Wang, J.; Moens, L.; Hensley, J. E. Recent Advances in Heterogeneous Catalysts for Bio-Oil Upgrading via “Ex Situ Catalytic Fast Pyrolysis”: Catalyst Development through the Study of Model Compounds. *Green Chem.* **2014**, *16*, 454–490.
- (3) Karadas, F.; Atilhan, M.; Aparicio, S. Review on the Use of Ionic Liquids (ILs) as Alternative Fluids for CO<sub>2</sub> Capture and Natural Gas Sweetening. *Energy Fuels* **2010**, *24*, 5817–5828.
- (4) Stanislaus, A.; Marafi, A.; Rana, M. S. Recent Advances in the Science and Technology of Ultra Low Sulfur Diesel (ULSD) Production. *Catal. Today* **2010**, *153*, 1–68.
- (5) Waernbaum, G.; Wallin, I. Hazards in the Work Environment—Hydrogen Sulfide: Spectrophotometric Determination of Hydrogen Sulfide. *Scand. J. Work, Environ. Health* **1979**, *5*, 31–34.
- (6) Guidotti, T. L. Hydrogen Sulphide. *Occup. Med.* **1996**, *46*, 367–371.
- (7) Chua, C. K.; Pumera, M. Susceptibility of FeS<sub>2</sub> Hydrogen Evolution Performance to Sulfide Poisoning. *Electrochem. Commun.* **2015**, *58*, 29–32.

(8) Tang, Q.-L.; Duan, X.-X.; Zhang, T.-T.; Fan, X.; Zhang, X. Comparative Theoretical Study of the Chemistry of Hydrogen Sulfide on Cu(100) and Au(100): Implications for Sulfur Tolerance of Water Gas Shift Nanocatalysts. *J. Phys. Chem. C* **2016**, *120*, 25351–25360.

(9) Hamon, L.; Serre, C.; Devic, T.; Loiseau, T.; Millange, F.; Férey, G.; De Weireld, G. Comparative Study of Hydrogen Sulfide Adsorption in the MIL-53(Al, Cr, Fe), MIL-47(V), MIL-100(Cr), and MIL-101(Cr) Metal-Organic Frameworks at Room Temperature. *J. Am. Chem. Soc.* **2009**, *131*, 8775–8777.

(10) Ethiraj, J.; Bonino, F.; Lamberti, C.; Bordiga, S. H<sub>2</sub>S Interaction with HKUST-1 and ZIF-8 MOFs: A Multitechnique Study. *Microporous Mesoporous Mater.* **2015**, *207*, 90–94.

(11) Zhang, C.; Lively, R. P.; Zhang, K.; Johnson, J. R.; Karvan, O.; Koros, W. J. Unexpected Molecular Sieving Properties of Zeolitic Imidazolate Framework-8. *J. Phys. Chem. Lett.* **2012**, *3*, 2130–2134.

(12) Son, W.-J.; Choi, J.-S.; Ahn, W.-S. Adsorptive Removal of Carbon Dioxide Using Polyethyleneimine-Loaded Mesoporous Silica Materials. *Microporous Mesoporous Mater.* **2008**, *113*, 31–40.

(13) Mueller, R.; Hariharan, V.; Zhang, C.; Lively, R.; Vasenkov, S. Relationship between Mixed and Pure Gas Self-Diffusion for Ethane and Ethene in ZIF-8/6FDA-DAM Mixed-Matrix Membrane by Pulsed Field Gradient NMR. *J. Membr. Sci.* **2016**, *499*, 12–19.

(14) Cotts, R. M.; Hoch, M. J. R.; Sun, T.; Markert, J. T. Pulsed Field Gradient Stimulated Echo Methods for Improved NMR Diffusion Measurements in Heterogeneous Systems. *J. Magn. Reson.* **1989**, *83*, 252–266.

(15) Kärger, J.; Ruthven, D. M.; Theodorou, D. N. *Diffusion in Nanoporous Materials*; Wiley-VCH Verlag GmbH & Co. KGaA: Weinheim, Germany, 2012.

(16) Blöchl, P. E. Projector Augmented-Wave Method. *Phys. Rev. B: Condens. Matter Mater. Phys.* **1994**, *50*, 17953–17979.

(17) Perdew, J. P.; Burke, K.; Ernzerhof, M. Generalized Gradient Approximation Made Simple. *Phys. Rev. Lett.* **1996**, *77*, 3865–3868.

(18) Grimme, S.; Antony, J.; Ehrlich, S.; Krieg, H. A Consistent and Accurate Ab Initio Parametrization of Density Functional Dispersion Correction (DFT-D) for the 94 Elements H–Pu. *J. Chem. Phys.* **2010**, *132*, 154104.

(19) Kresse, G.; Hafner, J. Ab Initio Molecular Dynamics for Liquid Metals. *Phys. Rev. B: Condens. Matter Mater. Phys.* **1993**, *47*, 558–561.

(20) Kresse, G.; Hafner, J. Ab Initio Molecular-Dynamics Simulation of the Liquid-Metal–Amorphous-Semiconductor Transition in Germanium. *Phys. Rev. B: Condens. Matter Mater. Phys.* **1994**, *49*, 14251–14269.

(21) Kresse, G.; Furthmüller, J. Efficiency of Ab-Initio Total Energy Calculations for Metals and Semiconductors Using a Plane-Wave Basis Set. *Comput. Mater. Sci.* **1996**, *6*, 15–50.

(22) Kresse, G.; Joubert, D. From Ultrasoft Pseudopotentials to the Projector Augmented-Wave Method. *Phys. Rev. B: Condens. Matter Mater. Phys.* **1999**, *59*, 1758–1775.

(23) Park, K. S.; Ni, Z.; Côté, A. P.; Choi, J. Y.; Huang, R.; Uribe-Romo, F. J.; Chae, H. K.; O’Keeffe, M.; Yaghi, O. M. Exceptional Chemical and Thermal Stability of Zeolitic Imidazolate Frameworks. *Proc. Natl. Acad. Sci. U.S.A.* **2006**, *103*, 10186–10191.

(24) Zhang, C.; Han, C.; Sholl, D. S.; Schmidt, J. R. Computational Characterization of Defects in Metal-Organic Frameworks: Spontaneous and Water-Induced Point Defects in ZIF-8. *J. Phys. Chem. Lett.* **2016**, *7*, 459–464.

(25) Chizallet, C.; Lazare, S.; Bazer-Bachi, D.; Bonnier, F.; Lecocq, V.; Soyer, E.; Quoineaud, A.-A.; Bats, N. Catalysis of Transesterification by a Nonfunctionalized Metal–Organic Framework: Acido-Basicity at the External Surface of ZIF-8 Probed by FTIR and Ab Initio Calculations. *J. Am. Chem. Soc.* **2010**, *132*, 12365–12377.

(26) Chizallet, C.; Bats, N. External Surface of Zeolite Imidazolate Frameworks Viewed Ab Initio: Multifunctionality at the Organic–Inorganic Interface. *J. Phys. Chem. Lett.* **2010**, *1*, 349–353.

(27) Tian, F.; Cerro, A. M.; Mosier, A. M.; Wayment-Steele, H. K.; Shine, R. S.; Park, A.; Webster, E. R.; Johnson, L. E.; Johal, M. S.; Benz, L. Surface and Stability Characterization of a Nanoporous ZIF-8 Thin Film. *J. Phys. Chem. C* **2014**, *118*, 14449–14456.

- (28) Moh, P. Y.; Cubillas, P.; Anderson, M. W.; Atfield, M. P. Revelation of the Molecular Assembly of the Nanoporous Metal Organic Framework ZIF-8. *J. Am. Chem. Soc.* **2011**, *133*, 13304–13307.
- (29) Zhu, Y.; Ciston, J.; Zheng, B.; Miao, X.; Czarnik, C.; Pan, Y.; Sougrat, R.; Lai, Z.; Hsiung, C.-E.; Yao, K.; Pinnau, I.; Pan, M.; Han, Y. Unravelling Surface and Interfacial Structures of a Metal-Organic Framework by Transmission Electron Microscopy. *Nat. Mater.* **2017**, *16*, 532–536.
- (30) Lively, R. P.; Dose, M. E.; Thompson, J. A.; McCool, B. A.; Chance, R. R.; Koros, W. J. Ethanol and Water Adsorption in Methanol-Derived ZIF-71. *Chem. Commun.* **2011**, *47*, 8667–8669.
- (31) Pang, S. H.; Han, C.; Sholl, D. S.; Jones, C. W.; Lively, R. P. Facet-Specific Stability of ZIF-8 in the Presence of Acid Gases Dissolved in Aqueous Solutions. *Chem. Mater.* **2016**, *28*, 6960–6967.
- (32) Zhang, C.; Gee, J. A.; Sholl, D. S.; Lively, R. P. Crystal-Size-Dependent Structural Transitions in Nanoporous Crystals: Adsorption-Induced Transition in ZIF-8. *J. Phys. Chem. C* **2014**, *118*, 20727–20733.
- (33) Han, C.; Zhang, C.; Tymińska, N.; Schmidt, J. R.; Sholl, D. S. Insights into the Stability of Zeolitic Imidazolate Frameworks in Humid Acidic Environments from First Principles Calculations. *J. Phys. Chem. C* **2018**, *122*, 4339–4348.
- (34) Semino, R.; Ramsahye, N. A.; Ghoufi, A.; Maurin, G. Microscopic Model of the Metal–Organic Framework/Polymer Interface: A First Step toward Understanding the Compatibility in Mixed Matrix Membranes. *ACS Appl. Mater. Interfaces* **2016**, *8*, 809–819.
- (35) Henkelman, G.; Uberuaga, B. P.; Jónsson, H. A Climbing Image Nudged Elastic Band Method for Finding Saddle Points and Minimum Energy Paths. *Chem. Phys.* **2000**, *113*, 9901–9904.
- (36) Henkelman, G.; Jónsson, H. Improved Tangent Estimate in the Nudged Elastic Band Method Minimum Energy Paths and Saddle Points. *Chem. Phys.* **2000**, *113*, 9978–9985.
- (37) Bhattacharyya, S.; Pang, S. H.; Dutzer, M. R.; Lively, R. P.; Walton, K. S.; Sholl, D. S.; Nair, S. Interactions of SO<sub>2</sub>-Containing Acid Gases with ZIF-8: Structural Changes and Mechanistic Investigations. *J. Phys. Chem. C* **2016**, *120*, 27221–27229.
- (38) Mounfield, W. P.; Han, C.; Pang, S. H.; Tumuluri, U.; Jiao, Y.; Bhattacharyya, S.; Dutzer, M. R.; Nair, S.; Wu, Z.; Lively, R. P.; Sholl, D. S.; Walton, K. S. Synergistic Effects of Water and SO<sub>2</sub> on Degradation of MIL-125 in the Presence of Acid Gases. *J. Phys. Chem. C* **2016**, *120*, 27230–27240.
- (39) Pusch, A.-K.; Splith, T.; Moschkowitz, L.; Karmakar, S.; Biniwale, R.; Sant, M.; Suffritti, G. B.; Demontis, P.; Cravillon, J.; Pantatosaki, E.; Stallmach, F. NMR Studies of Carbon Dioxide and Methane Self-Diffusion in ZIF-8 at Elevated Gas Pressures. *Adsorption* **2012**, *18*, 359–366.
- (40) Chmelik, C.; Freude, D.; Bux, H.; Haase, J. Ethene/Ethane Mixture Diffusion in the MOF Sieve ZIF-8 Studied by MAS PFG NMR Diffusometry. *Microporous Mesoporous Mater.* **2012**, *147*, 135–141.
- (41) ben-Avraham, D.; Havlin, S. *Diffusion and Reactions in Fractals and Disordered Systems*; Cambridge University Press: Cambridge, U.K., 2005.
- (42) Zhang, K.; Lively, R. P.; Zhang, C.; Koros, W. J.; Chance, R. R. Investigating the Intrinsic Ethanol/Water Separation Capability of ZIF-8: An Adsorption and Diffusion Study. *J. Phys. Chem. C* **2013**, *117*, 7214–7225.
- (43) Pampel, A.; Fernandez, M.; Freude, D.; Kärger, J. New Options for Measuring Molecular Diffusion in Zeolites by MAS PFG NMR. *Chem. Phys. Lett.* **2005**, *407*, 53–57.
- (44) Fernandez, M.; Pampel, A.; Takahashi, R.; Sato, S.; Freude, D.; Kärger, J. Revealing Complex Formation in Acetone-N-alkane Mixtures by MAS PFG NMR Diffusion Measurement in Nanoporous Hosts. *Phys. Chem. Chem. Phys.* **2008**, *10*, 4165–4171.
- (45) Gaillard, M.; Montouillout, V.; Mauge, F.; Fernandez, C. An Infrared and Solid-State NMR Study of the H<sub>2</sub>S Adsorption on Basic Zeolite. In *Recent Advances in the Science and Technology of Zeolites and Related Materials, Pts a–C*; VanSteen, E., Claeys, M., Callanan, L. H., Eds.; Elsevier, 2004; Vol. 154, pp 1679–1685.